ACS APPLIED POLYMER MATERIALS

pubs.acs.org/acsapm Article

Mastering Superior Performance Origins of Ionic Polyurethane/Silica Hybrids

Jean-Emile Potaufeux, Jérémy Odent,* Delphine Notta-Cuvier, Sophie Barrau, Chiara Magnani, Rémi Delille, Chunbo Zhang, Guoming Liu, Emmanuel P. Giannelis, Alejandro J. Müller, Franck Lauro, and Jean-Marie Raquez

Cite This: https://doi.org/10.1021/acsapm.1c01396 Read Online

ACCESS | Metrics & More | Article Recommendations | Supporting Information

ABSTRACT: Even though reversible interactions within ionic hydrogels are well-studied, underlying mechanisms responsible for the high-value added performance of ionic nanocomposites remain almost unexplored. We herein propose a fundamental understanding aiming at elucidating the mechanism behind the reversible breaking and reformation of ionic bonding in the case of organic−inorganic hybrids made of a combination of imidazolium-functionalized poly(ethylene glycol)-based polyurethane (*im*-PU) and surface-modified sulfonate silica nanoparticles (SiO_2−SO_3H). Such ionic hybrids already demonstrated unique features related to the presence of electrostatic interactions, but the underlying mechanisms governing the overall material performance have never been discussed. To dissociate the reinforcement role of nanoparticles and ionic interactions, either standard nonionic SiO_2 or ionic SiO_2−SO_3H nanoparticles were introduced into *im*-PU. Mechanical performances, thermal transitions, relaxation processes, and the morphology of the hybrids were deeply investigated to better comprehend the mechanisms at the origin of the ionic material reinforcement. In addition, a mechanistic investigation is proposed to quantify the dissipation energy ability of the as-proposed ionic hybrids, and an approach is presented to identify a characteristic time for restoration of reversible ionic bonds under different loading scenarios.

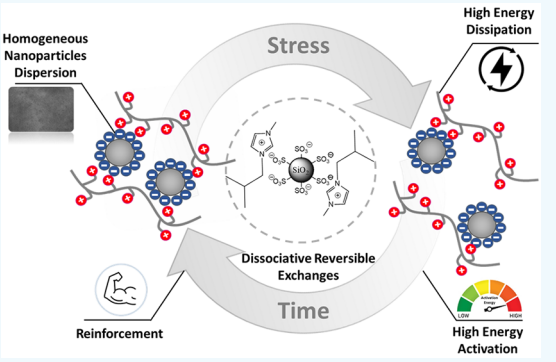

KEYWORDS: *ionic interactions, structure-to-properties relationships, ionic hybrids, mechanistics, reversible exchanges*

Dynamically reversible chemistries where specific bonds or interactions can undergo reversible breaking and restoration under certain conditions have gained extensive attention and opened up inspiring pathways for the design of tunable adaptive materials.[1] Owing to these attributes and reversibility, these materials have unique features including shape-memory, self-healing, stimuli-responsiveness, and adaptability.[2−6] A variety of dynamic interactions is noncovalent bonding represented by hydrogen bonding,[7] π−π stacking,[8] metal−ligand coordination,[9−11] hydrophobic association,[12] guest−host interactions,[13] and ionic bonding.[14−16] Among them, ionic systems differentiate from other dynamic polymeric materials as the resulting electrostatic interactions can be easily tuned and controlled by adequately choosing the nature, charge density, and ionic strength of ions and counterions.[17−19] While the behavior mechanism in ionic materials is not well understood, several mechanistic approaches have been performed on dual network (DN) hydrogels to model ionic interactions.[20−22] Such polymeric systems are excellent models to permit in-depth understanding of the breaking/reforming responses of ionically modified materials. As summarized in our recent review, investigations aiming at developing theoretical models to predict stress during loading−unloading cycles on the basis of experimental data were done.[23−26] Taking into account the reattachment of ionic cross-links after breaking and stress-dissipation, Hui and Long's model justified toughening and rate-dependent behaviors as well as self-healing ability.[23] Such a model gave access for the first time to the dissipation energy related to transient network rupture and was extendable to hydrogels containing multiple reversible interactions. Later, Long et al. established an enhanced model which included the strain history of the material as well as the attachment and detachment kinetics of ionic cross-links to perfectly fit loading−unloading experiment data and fully characterize the stress-dissipation process.[24] Other approaches have been explored to model large deformation viscoelastic responses[25] or to explain phenomenon such as Mullins effect (i.e., stress

Received: October 14, 2021
Accepted: October 25, 2021

softening)[27] and self-healing ability.[23,26] Still, shedding light on the fundamental mechanism underlying more advanced ionic polymeric materials is appealing, especially on these ionic nanocomposites.

Building on ionic motifs, our group recently designed ionic nanocomposites made of a combination of imidazolium-functionalized polymers and surface-modified sulfonate silica nanoparticles (SiO_2-SO_3H). The proximity of the imidazolium cationic sites to the anionic sulfonate groups allowed maximizing Coulomb interactions. Poly(ethylene glycol)-based polyurethane (*im*-PU) nanocomposites were thereby developed to combine the dynamic and reversible nature of ionic imidazolium-sulfonate interactions with the reinforcement ability of nanoparticles in nanocomposites.[28] As a result, stiff, tough and highly stretchable nanocomposite materials showing remarkable shape-recovery and self-healing behaviors were obtained. In addition, the nanocomposites exhibited unique strain-rate-dependent mechanical behavior (i.e., yield stress, Young's modulus and more uncommonly ultimate strain at break increased when increasing strain rate). Ionically modified silica nanoparticles are herein thought to play a crucial role in the overall material performance by creating multiple temporary cross-links between the imidazolium-functionalized polymer chains.[28] Recall that the inherent brittleness of polylactide (PLA) is a perpetual challenge for its industrialization, we further investigated some of the potential advantages of introducing electrostatic interactions into such system.[29] Integrating the resulting ionic *im*-PU/SiO_2-SO_3H systems into a conventional PLA matrix thereby promoted the emergence of greater energy dissipative toughening mechanisms under quasi-static and high loadings compared to neat PLA. Meanwhile, we showed that conventional, nonresponsive PLA can be endowed with shape-memory behavior by blending commercial PLA with imidazolium-terminated glassy PLA (*im*-PLA) and rubbery poly-[ε-caprolactone-*co*-D,L-lactide] (*im*-P(CL-*co*-LA) oligomers and adding SiO_2-SO_3H.[30] Yet, we believe the dissociation dynamics of the ionic imidazolium−sulfonate cross-links are responsible for the appealing performance of these as-designed materials. Although these contributions demonstrated some potential advantages of introducing electrostatic interactions in these hybrids, establishing the exact mechanism behind the ionic dissociation as well as delineating the key parameters responsible for the final material performance remain complex and challenging.

In the present contribution, we propose a fundamental understanding aiming at elucidating the underlying mechanisms behind the reversible breaking and reformation of ionic bonding in ionic organic−inorganic hybrids. Ionic *im*-PU/SiO_2-SO_3H nanocomposites are herein selected as a model system that leverage the reversible character of ionic bonds with the reinforcing effect of nanoparticles. The success of the material suggested multiple critical questions that we sought to address in this work: Can we precisely distinguish the contribution of the nanoparticles addition toward electrostatic interactions on the overall material performances? Is any change in crystallization behavior, in molecular mobility, or in the reversibility of the ionic cross-links the dominant mechanism responsible for the high-value added performance of ionic organic−inorganic hybrids?. First, the introduction of either standard nonionic SiO_2 or ionic SiO_2-SO_3H into *im*-PU is envisioned to precisely distinguish the contribution of the nanoparticles addition toward electrostatic interactions on mechanical performances, thermal transitions, morphology, and the crystallization process. Dielectric spectroscopy and the time−temperature superposition (TTS) principle applied to rheology highlight the role of ionic polymer/particle interactions on the material reinforcement based on relaxation and resistance to flow energy activation modifications, respectively. The present work also relies on a mechanistical approach to fully characterize these reversible ionic interactions and explain the energy dissipation process underpinning, while proposing a strategy to approach the characteristic time of ionic interactions to rebond after deformation and rupture. The deeper understanding of dynamic interactions within ionic nanocomposites might help one to precisely design more advanced dynamic nanocomposites in the near future.

EXPERIMENTAL SECTION

Materials. Hexamethylene diisocyanate (HMDI, > 98%, Aldrich) was stored in a glovebox. Polyethylene glycol (PEG, 2000 g·mol^{-1}, Alfa Aesar), 2,2-bis(bromomethyl)propane-1,3-diol (BBPDO, 98%, Sigma), 1-methyl-imidazole (99%, Aldrich), dibutyltin dilaurate (DBTDL, 95%, Sigma), Ludox HS30 colloidal silica (mean diameter 18 nm, Aldrich), 3-(hydroxysilyl)-1-propanesulfonic acid (SIT, 40 wt %, Gelest), sodium hydroxide solution (1 M, Aldrich), anhydrous tetrahydrofuran (THF, >99.8%), and anhydrous *N*,*N*-dimethylformamide (DMF, >99.7%, Alfa Aesar) were used without further purification.

Synthesis of Imidazolium-Based Diol. Here, 1 equiv of BBPDO and 2.5 equiv of 1-methylimidazole were dissolved in a minimum volume of dry THF into a glass flask and refluxed at 65 °C for 24 h under stirring. After reaction, the imidazolium-based diol was recovered by solvent evaporation under vacuum (yield ≈ 83).

Ionic Nanocomposite Preparation. Imidazolium-functionalized poly(ethylene glycol)-based polyurethane (*im*-PU, $M_n \approx 95\,000$ g·mol^{-1}, Đ ≈ 2.6, yield ≈ 95%) and surface-modified sulfonate silica nanoparticles (*ca.* 17 ± 5 nm of diameter, 1 ± 0.1 mmol of SO_3H/g of silica) were prepared according to a previously reported procedure.[27] Briefly, imidazolium-functionalized polyurethanes were synthesized by the reaction of 1.2 equiv of hexamethylene diisocyanate with 0.9 equiv of polyethylene glycol oligomer, 0.1 equiv of imidazolium-based diol, and catalytic amounts of dibutyltin dilaurate in anhydrous DMF at 65 °C for 6 h under nitrogen. The imidazolium-functionalized polyurethane was recovered by precipitation into a 10-fold excess of diethyl ether, followed by filtration and drying under vacuum. The as-synthesized im-PU was dissolved in deionized water followed by the dropwise addition of the sulfonate silica suspension under stirring, sonication and freeze-drying to form ionic *im*-PU/SiO_2-SO_3H hybrids. The resulting materials were shaped into films by compression molding at 60 °C using the following procedure: no pressure for 2 min followed by three degassing steps and 1 min under 10 bar. The ^{1}H NMR spectra ($CDCl_3$, δ, ppm) at 7.44 (1H, s, −N−CH−N−) as well as 6.88 and 7.06 ppm (2H, s, −N−CHCH−N−) confirmed the incorporation of imidazolium moieties into the polymers. FTIR analyses and suitable physical pictures of resulting materials are provided in Figure S1 in the Supporting Information.

Characterization Techniques. Proton nuclear magnetic resonance (^{1}H NMR) spectra were recorded in DMSO, using a Bruker AMX-500 spectrometer at a frequency of 500 MHz. Size-exclusion chromatography (SEC) were carried out on an Agilent 1200 apparatus in THF (containing 2 wt % of NEt3). Samples in solution (1 mg·mL^{-1}) were injected with a 1 mL·min^{-1} flow rate at 35 °C in a precolumn PL gel 10 mm (50 × 7.5 mm) followed by two gradient columns PL gel 10 mm mixed-B (300 × 7.5 mm). Molecular weights and molecular weight distributions were calculated by reference to a relative calibration curve made of polystyrene standards. Dynamic mechanical thermal analyses (DMTA) were performed under ambient atmosphere using a DMTA Q800 apparatus from TA Instruments in a tension film mode. The measurements were carried out at a constant

https://doi.org/10.1021/acsapm.1c01396
ACS Appl. Polym. Mater. XXXX, XXX, XXX−XXX

frequency of 1 Hz, an amplitude of 15 μm and a temperature range from −80 to +70 °C at a heating rate of 2 °C·min^{-1}. Thermal gravimetric analyzes (TGA) were performed using a TGA Q500 from TA Instruments at a heating rate of 20 °C·min^{-1} from room temperature to 800 °C, under nitrogen flow. Differential scanning calorimetry (DSC) were performed on a DSC Q200 from TA Instruments using a heat−cool-heat method scanning from −80 to +80 °C at a heating and cooling rate of 10 °C·min^{-1}. Tensile tests were carried out on a Zwick universal tensile testing machine (speed = 100 mm·min^{-1}, preload = 1 N) on rectangular films (thickness ∼ 0.4 mm). After testing at 100 mm/min, samples were reheated using a hairdryer during few seconds, and original shape of the sample was recovered. Samples were then tested again for 3 cycles. Scanning transmission electron microscopy (STEM) experiments were performed on scanning electronic microscope Philips XL at an accelerated voltage up to 30 kV and various magnitudes. The sample films (70−80 nm thick) were previously prepared with a Leica UCT ultracryomicrotome by cutting at −100 °C.

Shape-Memory Behavior. Shape-memory tests were performed using a DMTA TA Q800 from TA Instruments in tension film mode under force-controlled mode. Rectangular specimens (approximately 25 × 5 x 0.5 mm^3) were cut from compression molded films. The shape-memory behavior was characterized using a four-step program as follows: (1) deformation, the sample is elongated by applying a given load (stress ramp of 0.05 MPa/min until ca. 0.1 MPa, and strain around 100%) at a temperature higher than the melting temperature of *im*-PU (T_m ∼ 60 °C); (2) fixing, the sample is cooled to 0 °C under a constant load; (3) unloading, the load is removed within 2 min (at intervals of 0.05 MPa until 0 MPa); and (4) recovery, the sample is heated to 60 °C at a rate of 2 °C/min. Shape-fixation (R_f) and shape-recovery (R_r) ratios were calculated using the following equations:[31]

$$R_f = \frac{\varepsilon_{un}}{\varepsilon_{ext}} R_r = \frac{\varepsilon_{un} - \varepsilon_f}{\varepsilon_{ext}}$$

where ε_{ext} is the maximum strain before stress release, ε_{un} is the strain after cooling and unloading, and ε_f is the final strain after heating during the recovery step.

Dielectric Spectroscopy. Dielectric relaxation measurements were performed on a Broadband Dielectric Spectrometer (Novocontrol Technologies) using samples of 25 × 25 mm^2 placed between two gold-plated electrodes (diameter of 20 mm). The complex permittivity $\varepsilon^*(f) = \varepsilon\cdot(f) - i\varepsilon''(f)$, with ε' the storage permittivity and ε'' the loss permittivity, was measured in the frequency range [10^{-1}−10^6 Hz] using an Alpha Analyzer. Samples were analyzed at different temperatures from −60 to +60 °C with a step of 5 °C. Temperature stabilization phase was done at each temperature step. Each relaxation was fitted with Havriliak−Negami function:

$$\varepsilon^* = \varepsilon_\infty + \frac{\varepsilon_0 - \varepsilon_\infty}{(1 + (i\omega\tau_{HN})^{\alpha HN})^{\beta HN}}$$

with ε^* the complex dielectric permittivity, ε_0 and ε_∞ the permittivity at low and high frequency limits respectively, τ_{HN} the relaxation time, and α_{HN} and β_{HN} the parameters describing the distribution of relaxation times, i.e., respectively the symmetric and asymmetric broadening of the complex dielectric response. Relaxation times τ_{HN} related to α and β relaxation were then obtained from the fit of the dielectric loss spectra. Vogel−Filcher−Tammann (VFT) and Arrhenius equations were used to fit the relaxation time related to respectively α-relaxation and β-relaxation:

$$\text{VFT: } \tau_{HN} = \tau_0 e^{-E_a/R(T-T_0)}$$

$$\text{Arrhenius: } \tau_{HN} = \tau_0 e^{-E_a/RT}$$

where τ corresponds to the relaxation time, τ_0 is the pre-exponent factor, E_a is the activation energy, T is the temperature, T_0 is the Vogel-temperature ($T_0 < T_g$), and R is the universal gas constant.[32]

Time−Temperature Superposition (TTS). Rheological measurements were performed using an Anton Paar Rheometer MCR-302 using a plate−plate geometry system with a 25 mm diameter. Frequency sweep measurements using time temperature superposition (TTS) were performed from 50 to 100 °C with a step of 10 °C (temperature stabilization of 5 min), a strain of 1% and a frequency range between 0.1 and 100 Hz. Horizontal shift factors a_T were applied in order to overlap curves along the reference temperature (arbitrary selected as 70 °C) and obtain mastercurves.[33] Note that no vertical shift factors b_T were applied here. Arrhenius equation was used in order to determine activation energies by fitting evolution of a_T with the temperature:

$$\ln(a_T) = \frac{E_a}{R}\left(\frac{1}{T} - \frac{1}{T_{ref}}\right)$$

where E_a is the activation energy, R the universal gas constant, T the temperature, and T_{ref} the reference temperature (here, T_{ref} = 70 °C). Meanwhile, the Williams−Landel−Ferry (WLF) equation was used to try to fit shift factors:

$$\ln(a_T) = \frac{-C_1^*(T - T_{ref})}{C_2 + (T - T_{ref})}$$

Here C_1 and C_2 are the empirical factors, T is the temperature, and T_{ref} is the reference temperature.[33]

Small-Angle X-ray Scattering (SAXS). Small-angle X-ray scattering (SAXS) experiments were carried out on the beamline 1W2A at the Beijing Synchrotron Radiation Facility (BSRF).[34] The wavelength of the X-ray radiation was 1.54 Å. The detector was Pilatus 1 M (DECTRIS), which contains 981 × 1043 pixels with a pixel size of 172 × 172 μm^2. The exposure time for the sample was 10 s for each sample. The sample to detector distance was 2862 mm. Intensity profiles were obtained by averaging the two-dimensional (2D) patterns by Fit2D package. SAXS curves of nanocomposites were fitted by polydisperse spheres combining with a structure factor with an attractive potential (stickyhardsphere in SASview).[35]

$$I(q) = P(q) \times S(q)$$

The model assumes a potential among the particles:

$$U(r) = \begin{cases} \infty, & r < \sigma \\ -U_0, & \sigma \le r \le \sigma + \Delta \\ 0, & r > \sigma + \Delta \end{cases}$$

where σ is the diameter of the sphere (σ = 2R), Δ is the width of the square well, and U_0 is the depth of well in units of kT. Similar parameters were used for SAXS measurements during tensile testing. Samples were stretched at a strain-rate of 10 mm·min^{-1} up to 50% of strain, then held for 1 min and finally unloaded up to 0 N. Images were taken before stretching and after each step. Note that the scattering signal from the neat *im*-PU has been subtracted from the nanocomposites.

Mechanistic Investigations. Samples for mechanistic investigation were cut from compression-molded films into dog-bone specimens (ASTM D638). Loading−unloading uniaxial cycles were performed at room temperature using an Instron E3000 electromagnetic tensile machine. Different loading and unloading speeds (1, 10, or 100 mm·min^{-1}) were applied, with a maximum stretching of 50% strain for *im*-PU and 20, 40, or 60% strain for polypropylene composite loaded with talc particles and elastomeric nodules. Loading−unloading tests were monitored using a Manta G camera (12.4 Mpx, 4112 × 3008 resolution) at a frame rate of 1 fps or 12 fps for the lowest or highest test speed, respectively. For some measurements, a holding time (up to 15 min) was imposed between loading and unloading steps. Digital Image Correlation (DIC) was used to extract true local strains on the zone of interest (ZOI) thanks to the tracking of a black and white speckle deposited in specimen surface.[36] VIC 2D software was used for the DIC as well as Matlab for further analysis of data.

https://doi.org/10.1021/acsapm.1c01396
ACS Appl. Polym. Mater. XXXX, XXX, XXX−XXX

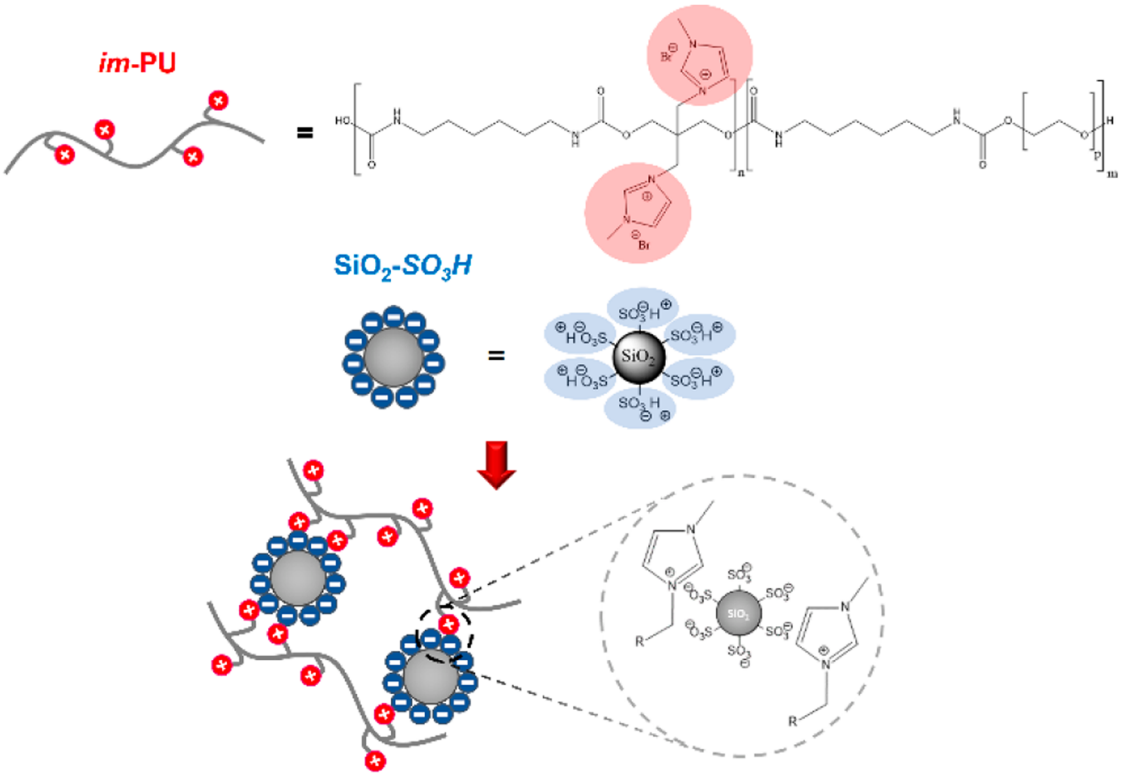

Figure 1. Ionic nanocomposites synthesized via self-assembly of *im*-PU and SiO_2-SO_3H that leverage Coulomb interactions.

RESULTS AND DISCUSSION

Rheological Behavior and Dielectric Relaxation. Ionic organic−inorganic hybrids that leverage the electrostatic interactions of imidazolium-functionalized poly(ethylene glycol)-based polyurethanes (*im*-PU, *ca.* 0.1 mmol·g^{-1}) and surface-modified sulfonate silica nanoparticles (SiO_2-SO_3H, *ca.* 1 mmol.g^{-1}) are purposely fabricated (Figure 1). Rheologically, the materials transition from liquid-like to solid-like behavior as the concentration of SiO_2-SO_3H increases (Figure S2 in the Supporting Information). The loss factor tan(δ) is frequently independent from 10 wt % of SiO_2-SO_3H, confirming the creation of an extensive 3D network of silica nanoparticles within the material at this loading. Herein, 10 wt % of SiO_2-SO_3H is required for theoretically achieving the neutralized charge balance (i.e., 1:1 ratio of sulfonate:imidazolium), so maximizing Coulomb interactions. In such systems, substituting ionic SiO_2-SO_3H by standard nonionic SiO_2 is envisioned to precisely distinguish contributions of the nanoparticle addition toward electrostatic interactions on the mechanism behind the high-value added performance of ionic nanocomposites. Rheological measurements show that adding either nonionic SiO_2 or ionic SiO_2-SO_3H nanoparticles within *im*-PU leads to an increase of the storage modulus in the lower frequency regime that can be attributed to the formation of a physical nanofiller network (Figure S3 in the Supporting Information).[37] Though, the addition of ionic SiO_2-SO_3H nanoparticles leads to higher storage modulus at low frequencies and a nearly frequency-independent loss factor (Winter−Chambon criterion), confirming the presence of ionic imidazolium-sulfonate interactions as well as the establishment of an extensive 3D network of silica nanoparticles within the material at such silica loading.[28]

Applying the time temperature superposition (TTS) principle shows an excellent superposition of data, confirming that the materials do not change (chemically or physically) during the rheological measurement (Figure 2).[38] Reporting the evolution of horizontal shift factors (a_T) with the temperature demonstrates that these materials follow an Arrhenius law in the temperature range of 50 to 100 °C (Figure 3). Meanwhile, the data do not fit with the Williams−Landel−Ferry law (Figure S4 and Table S1 in the Supporting Information), suggesting that the viscoelastic properties are rather governed by thermally activated processes than volume processes.[39] Arrhenius equation thereby provides the best overview of dynamic properties and gives access to activation energy E_a, which is herein proportional to the energy required to break and reform ionic interactions.[40] While neat *im*-PU has an activation energy of 35 kJ mol^{-1}, adding nonionic SiO_2 reduces this energy to 29 kJ mol^{-1}. It is commonly known that filler addition lowers E_a due to the reduction of cohesion within the final material. In contrast, adding ionic SiO_2-SO_3H to generate the ionic hybrid leads to significant increase of the activation energy up to 42 kJ mol^{-1}, that we ascribe to the formation of ionic sulfonate-imidazolium interactions in the system, thus reinforcing the overall material performance.

Similar evolutions of activation energy have been observed by performing dielectric spectroscopy measurements (Figure S5 in the Supporting Information). From low to high temperature, the β-relaxation process is first well-recognized and followed by the appearance of α-relaxation (while β-relaxation disappears), suggesting a type B glass former (Figure S6 in the Supporting Information).[41] While the α-relaxation corresponds to a large-scale rearrangement of *im*-PU segments, the β-relaxation is associated with the local mode, i.e., segmental motions from the amorphous *im*-PU chains.[42,43]

https://doi.org/10.1021/acsapm.1c01396
ACS Appl. Polym. Mater. XXXX, XXX, XXX−XXX

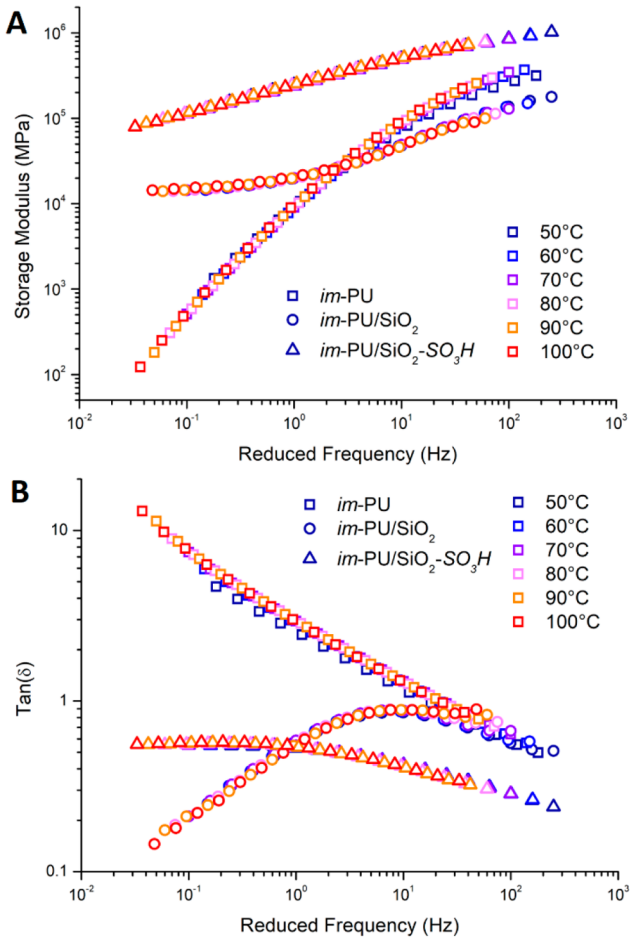

Figure 2. Application of TTS principle to rheology data (storage modulus (A) and tan δ (B)) of neat *im*-PU (squares), nonionic *im*-PU/SiO_2 hybrid (circles), and ionic *im*-PU/SiO_2–SO_3H hybrid (triangles).

Using Havriliak–Negami fitting (see Experimental Section), β-relaxation presents lower relaxation times over a large range of temperature compared to α-relaxation (Figure 4). While relaxation times of both α and β-relaxations decrease upon

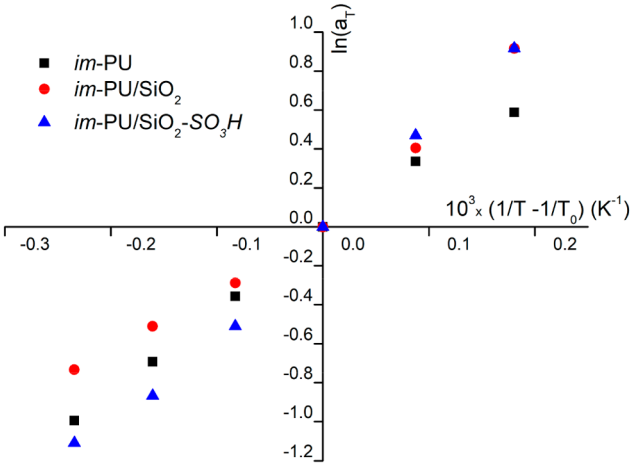

Figure 3. Arrhenius plots derived from TTS shift factors of neat *im*-PU (black, squares), nonionic *im*-PU/SiO_2 hybrid (red, circles), and ionic *im*-PU/SiO_2–SO_3H hybrid (blue, triangles).

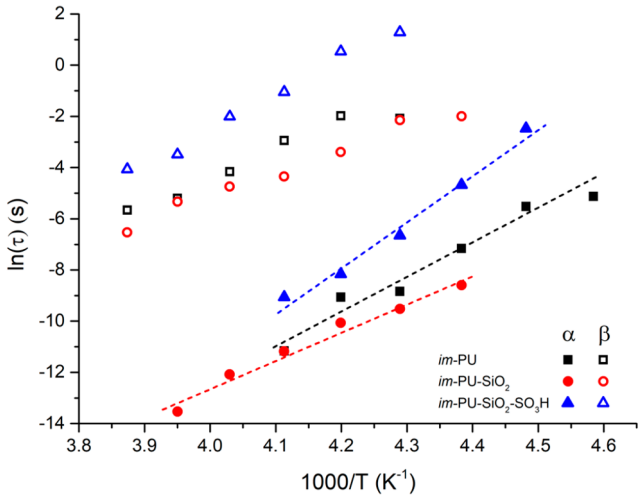

Figure 4. Activation energy of α (open dots) and β (solid dots) relaxations derived from dielectric spectroscopy of neat *im*-PU (black, squares), nonionic *im*-PU/SiO_2 hybrid (red, circles), and ionic *im*-PU/SiO_2–SO_3H hybrid (blue, triangles).

the addition of nonionic SiO_2, a significant increase is observed when silica nanoparticles are ionically modified (i.e., SiO_2–SO_3H). Few authors have already reported that the reduction of α-relaxation time upon the addition of conventional nanofillers (such as SiO_2) is due to restricted polymer chains mobility.[43] In contrast, the reduction of β-relaxation time is often related to an enhanced brittleness of the material, which is confirmed by mechanical investigations (see nonionic *im*-PU/SiO_2, Table 1). While the increase of β-relaxation time with the addition of nanofillers (as observed for ionic *im*-PU/SiO_2–SO_3H, see Figure 4) has never been clearly explained,[44] we attribute this phenomenon to the presence of electrostatic interactions in the system which toughen the material without strongly affecting the *im*-PU polymer chain mobility. Classic determination of the activation energy for α-relaxation using Vogel–Fulcher–Tammann (VFT) model (see Experimental Section) is herein impossible due to the narrow temperature range (i.e., 233 to 258 K) and the overlay within the conductivity contribution at high temperature and low frequency.[45] Yet, the activation energy associated with β relaxations is obtained through Arrhenius fitting (see Figure 4). That is, activation energy E_a of nonionic *im*-PU/SiO_2 and ionic *im*-PU/SiO_2–SO_3H hybrids are respectively lowered (ca. 91 kJ mol^{-1}) and enhanced (ca. 151 kJ mol^{-1}) compared to neat *im*-PU (*ca.* 107 kJ mol^{-1}). Thereby, the presence of reversible ionic interactions between polymer chains and silica nanoparticles is thought to be responsible for the more cohesive properties of the resulting ionic hybrid.

Morphology and Crystallization. Small-angle X-ray scattering (SAXS) experiments are performed in order to measure the level of dispersion of either standard nonionic SiO_2 and ionic SiO_2–SO_3H nanoparticles within *im*-PU matrix. Figure 5 compares the intensity profiles $I(q)$. Neat *im*-PU presents a maximum of intensity at 0.048 $Å^{-1}$ related to its average long-period, i.e. the stacking of amorphous layers and crystalline lamellae. The long-period is thereby estimated by using Bragg's equation (Lp = $2\pi/q_{max}$) at 13.1 nm in accordance with previous observations.[29] Adding either standard nonionic SiO_2 or ionic SiO_2–SO_3H nanoparticles into *im*-PU lead to greater intensity due to the high stiffness

https://doi.org/10.1021/acsapm.1c01396
ACS Appl. Polym. Mater. XXXX, XXX, XXX–XXX

Table 1. Thermomechanical Properties of Neat *im*-PU, Non-Ionic *im*-PU/SiO_2 Hybrid, and Ionic *im*-PU/SiO_2−SO_3H Hybrid[a]

sample	E [MPa]	σ_y [MPa]	ε_b [%]	E_{def} [MJ·m^{-3}]	T_c [°C]	ΔH_c [J·g^{-1}]
im-PU	230	11.4	1600	210	19.8	71
im-PU/SiO_2	370	7.0	3	0.1	21.5	87
im-PU/SiO_2−SO_3H	270	12.1	1600	240	22.8	64

[a]Key: E, Young's modulus; σ_y, yield stress; ε_b, strain at break; E_{def}, volume strain energy dissipated under tensile testing; T_c, crystallization temperature; ΔH_{cryst}, crystallization enthalpy

contrast between the nanoparticles and the polymer matrix. Although the volume concentration of silica nanoparticles is low within *im*-PU matrix (*ca.* 5.5 vol % related to 10 wt %), SAXS profiles do not fit to sphere form factor as one would expect for spherical silica nanoparticles. Though, at small q, i.e., within the Guinier region, a relationship of $I \sim q^2$ is observed for both nonionic *im*-PU/SiO_2 and ionic *im*-PU/SiO_2−SO_3H nanocomposites. In contrast, a potential energy corresponding to a thickness of *ca.* Δ = 8 Å and a depth of ca. U_0 = 3 kT is extracted by fitting with polydisperse spheres combining a structure factor with an attractive potential model (see the Experimental Section). The fitting further indicates an average radius of silica nanoparticles of 80 Å with a polydispersity of 0.13 assuming a Gaussian size distribution consistent with monodisperse silica nanoparticles of ca. 17 ± 5 nm. Though, there are small differences between the SAXS profiles of nonionic *im*-PU/SiO_2 and ionic *im*-PU/SiO_2−SO_3H nanocomposites. That is, the low-q region of the scattering curve is characteristic for the overall dimension of the particle within the polymer matrix. In this region, the decrease of the slope of the fit to the Guinier region for the ionic *im*-PU/SiO_2−SO_3H hybrid reflects higher levels of dispersion of the nanoparticles in the polymer. Besides, STEM measurements show the ionic nanocomposites to be size-homogeneous and well dispersed which we attribute to the presence of electrostatic interactions in the system (Figure S7 in the Supporting Information). We also found that the particle dispersion is not affected under mechanical loadings with no clear appearance of particle aggregation or modification of form factor in SAXS profiles (Figure S8 in the Supporting Information).

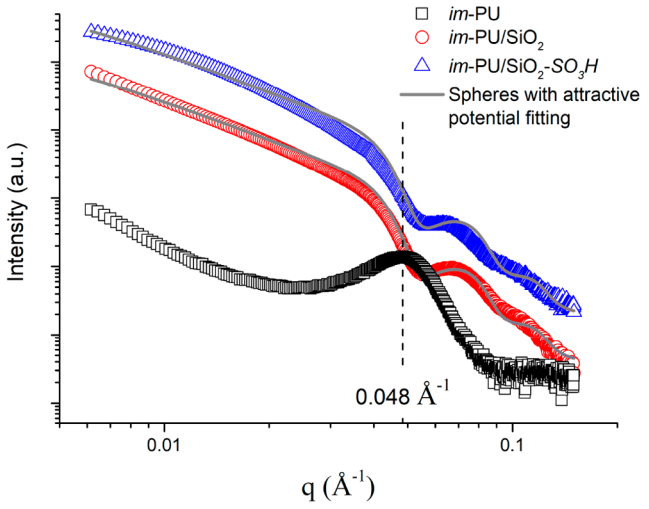

Figure 5. SAXS profiles and fitting curves of neat *im*-PU (squares), nonionic *im*-PU/SiO_2 hybrid (circles), and ionic *im*-PU/SiO_2−SO_3H hybrid (triangles).

It is well-known that nanoparticles can further act as nucleating agent, thus amplifying the crystallization of any polymeric materials.[46] Overall, adding either nonionic SiO_2 or ionic SiO_2−SO_3H nanoparticles within *im*-PU impact the crystallinity (Table 1 and Figure S9 in the Supporting Information), crystal nucleation (Figure S10 and Figure S11 in the Supporting Information) and growth (Figure S12 in the Supporting Information) of *im*-PU matrix (Figure S10 in the Supporting Information). Though, differences in crystallization behavior between nonionic *im*-PU/SiO_2 and ionic *im*-PU/SiO_2−SO_3H nanocomposites are observed. That is, the ionic *im*-PU/SiO_2−SO_3H hybrid leads to crystallization at higher temperature but of lower enthalpy compared to nonionic *im*-PU/SiO_2 hybrid (Table 1 and Figure S9 in the Supporting Information). On the other hand, crystallization kinetics reveal that induction time (Figure S10 in the Supporting Information) and half-time (Figure S11 in the Supporting Information) of crystallization of the ionic *im*-PU/SiO_2−SO_3H hybrid are superior to the nonionic *im*-PU/SiO_2 hybrid. Meanwhile, the growth rates of spherulites for ionic *im*-PU/SiO_2−SO_3H (i.e., characterized by numerous tiny-size spherulites) is slower than nonionic *im*-PU/SiO_2 (i.e., characterized by a few large-size spherulites) and neat *im*-PU (Figure S12 in the Supporting Information). The latter results suggest that the presence of imidazolium-sulfonate ionic interactions in the system hinder the crystallization process. Since the nanoparticles and polymer chains carry multiple ionic groups (i.e., SiO_2−SO_3H, *ca.* 1 mmol·g^{-1}; *im*-PU, *ca.* 0.1 mmol·g^{-1}), it is reasonable to speculate that these strong polymer−particle interactions seriously hinder the chain mobility, resulting in enhanced suppression of crystallization.[47]

Thermal Stability and Mechanical Response. At first sight, adding either standard nonionic SiO_2 or ionic SiO_2−SO_3H into *im*-PU matrix leads to an increase of storage modulus on DMTA temperature sweep profiles (Figure S13 in the Supporting Information). While neat *im*-PU and nonionic *im*-PU/SiO_2 reveal a drop of moduli at *ca.* 42 °C (i.e., melt temperature of *im*-PU), ionic *im*-PU/SiO_2−SO_3H does not flow but rather displays a slight softening at *ca.* 45 °C followed by a plateau at higher temperature. We believe that the extensive 3D network resulting from ionic interactions between anionic sulfonate sites at the silica nanoparticle surface and cationic imidazolium groups attached onto the highly functionalized *im*-PU is responsible for these properties. Typical dissociative noncovalent dynamic systems usually show no plateau as the continuous rupture/reformation of the 3D network allows the polymeric material to flow.[48,49] Our unexpected result is herein explained by the presence of strong ionic interactions (*ca.* imidazolium−sulfonate interactions) and the reduced molecular mobility of nanocomposites is further approached by tensile investigations (Table 1). While the significant increase in modulus is typically accompanied by a decrease in elongation at break and mechanical dissipated energy (i.e., area under the stress−strain

https://doi.org/10.1021/acsapm.1c01396
ACS Appl. Polym. Mater. XXXX, XXX, XXX−XXX

curve) in nonionic *im*-PU/SiO_2 hybrid, the ionic *im*-PU/SiO_2–SO_3H hybrid reveals simultaneous improvement in stiffness and energy dissipation compared to neat *im*-PU. Recall that the only difference between both nanocomposites is the surface functionalization of silica nanoparticles with anionic sulfonate moieties that endow the system with reversible dynamic ionic interactions. All in all, the ionic nanocomposite not only possesses exceptional mechanical performance but further exhibits unique shape-memory features (Figure S14 in the Supporting Information). While neat *im*-PU and nonionic *im*-PU/SiO_2 did not possess any shape-memory ability, the ionic *im*-PU/SiO_2–SO_3H presented fixity ratio of *ca.* R_f = 100% and a recovery ratio of *ca.* R_r = 78% ($T_{act.} > T_m \approx 37$ °C). They are further mechanically robust after multiple rounds of thermal reprocessing or recycling (Figure S15 in the Supporting Information).

Mechanistic Understanding and Underlying Mechanism. It is commonly established that the reversible nature of ionic cross-links confers strain-rate dependent behaviors to ionic polymeric materials.[20,50,51] Unlike the vast majority of studies available in literature, loading–unloading cyclic tests at different strain rates using the "true axial deformation" from camera acquisition and Digital Image Correlation (DIC) post-treatment instead of the "machine deformation" (i.e., computed from jack displacement) are herein performed, thus providing the true response of the material to mechanical loads (i.e., including internal inertia or Mullins effect).[36] While nonionic *im*-PU/SiO_2 nanocomposite displays very limited plastic deformation and inherent brittleness (see Table 1), ionic *im*-PU/SiO_2–SO_3H nanocomposite dissipates *ca.* 3 times more energy than neat *im*-PU upon successive loading–unloading cycles (Figure 6 and Table S2 in the Supporting Information). We attribute this large energy dissipation to the dissociation dynamics of ionic imidazolium-sulfonate interactions present in the system with the reinforcement ability of nanoparticles in nanocomposites. Besides, the ability of neat *im*-PU to dissipate energy decreases with the succession of cycles caused by local damage that progressively weakened the material (Table S2 in the Supporting Information). In contrast, the ionic *im*-PU/SiO_2–SO_3H nanocomposite does not show any significant drop of energy dissipation when repeatedly stretched to large deformation. We believe that electrostatic interactions can selectively undergo reversible breaking and restoration upon repeated loadings, thus limiting irreversible damage.[52]

Based on several mechanistic studies performed on DN hydrogels, it is well-documented that the breakage of the reversible ionic bonds is sensitive to strain-rate during the loading process.[22,24,25,53] Whereas during unloading, the mechanical response is not sensitive to the strain-rate because there is no breakage of the reversible ionic interactions during the unloading process. Typically, increasing the strain rate leads to a decrease of dissipated energy for neat *im*-PU. In contrast, the ionic *im*-PU/SiO_2–SO_3H nanocomposite can not only sustain much higher level of strain but also shows a higher energy dissipation ability at higher strain-rate, in accordance with previous observations published by Odent et al. (Figure S16 and Table S3 in the Supporting Information).[28] Unlike loading, unloading does not affect the amount of dissipated energy since no additional breakage occurs during this step. We attribute the mechanism by which the ionic nanocomposite dissipates strain energy to the dynamic exchanges

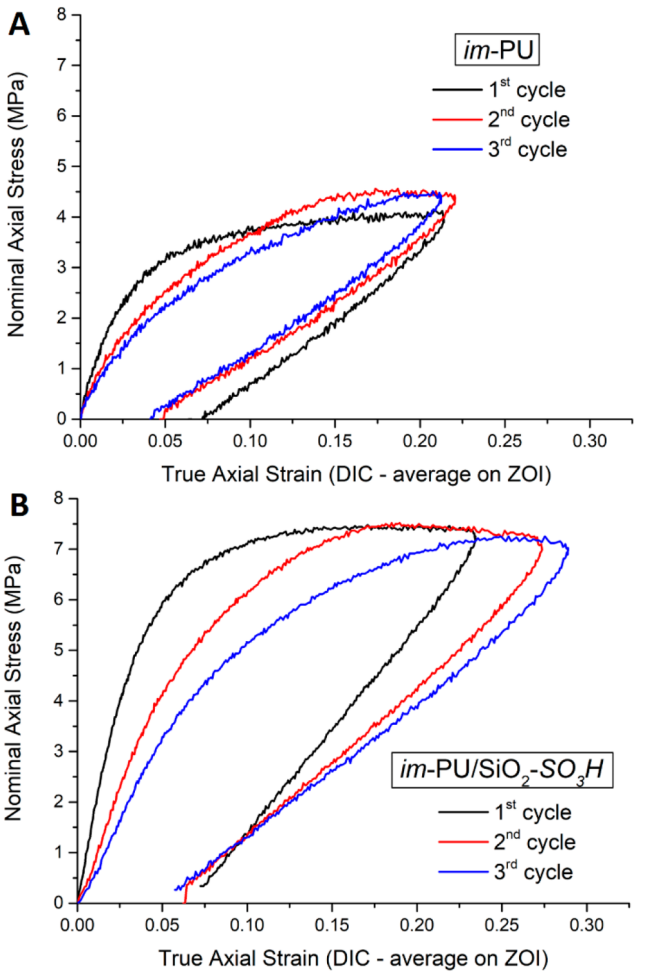

Figure 6. Mechanical behavior under successive cycle loadings of (A) neat *im*-PU and (B) ionic *im*-PU/SiO_2–SO_3H hybrid (50% strain; strain rate of 10 mm·min^{-1}).

of the ionic cross-links[20,24] as well as motion of the nanoparticles under applied stress.[54,55]

Stress–relaxation measurements where loading and unloading phases are separated by a holding time at constant stretching readily allow determining the time needed for reversible ionic interactions to reform (Figure 7). Defining the evolution of apparent modulus during the unloading process (via the slope of stress–strain curves) further allows to estimate damage in materials. For instance, a conventional polypropylene-based composite exhibits greater irreversible damages at higher loadings (Figure S17 in the Supporting Information) as indicated by a decrease of apparent modulus during unloading. In addition, the resulting material is not affected by the holding time on residual strain generation during the cyclic mechanical stimulation (Figure S18 in the Supporting Information). Therein, only specimens that experienced similar level of damage before the holding period to ensure similar maximum true axial strain are strictly compared. As a result, ionic *im*-PU/SiO_2–SO_3H hybrids that experienced a holding time of 2s and 10s are paired together, whereas holding periods of 30s and 5 min forms another pair (Figure 7). During unloading, the apparent modulus of the ionic *im*-PU/SiO_2–SO_3H hybrid is expected to increase with the holding time likely owing to the restoration of the ionic cross-links. Still, no significant difference is observed in

https://doi.org/10.1021/acsapm.1c01396
ACS Appl. Polym. Mater. XXXX, XXX, XXX–XXX

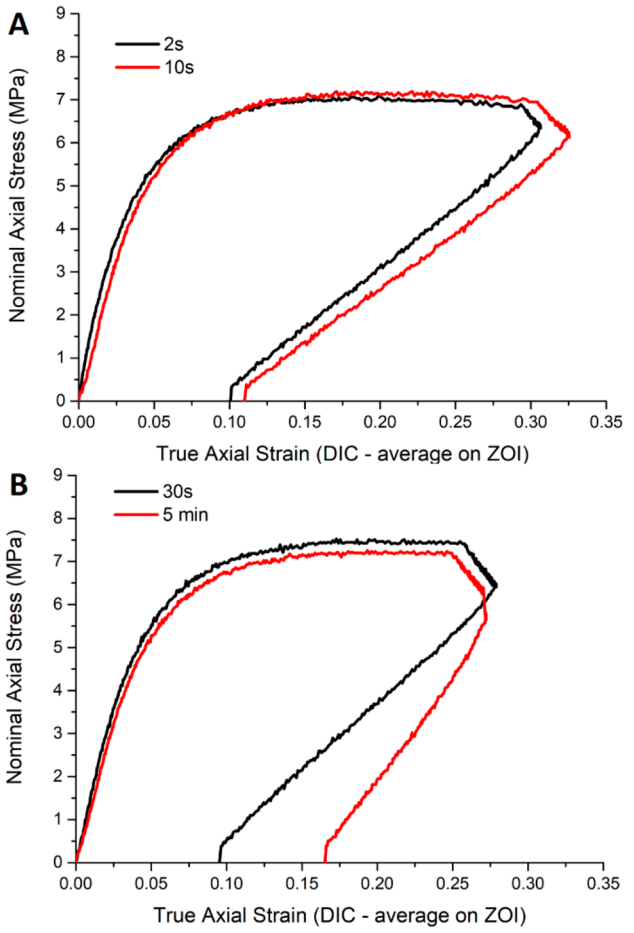

Figure 7. Stress−strain curves (50% strain; strain rate of 10 $mm.min^{-1}$) related to cyclic measurements of ionic *im*-PU/SiO_2−SO_3H hybrid at different holding times: (A) 2 s vs. 10 s and (B) 30 s vs. 5 min.

specimens that are held during 2, 2, and 10 s which indicates too short holding times to recover the physical ionic network (Figure 7A). In contrast, a stiffening effect is clearly evidenced when the ionic *im*-PU/SiO_2−SO_3H hybrids experienced a holding time of 5 min, which we assume resulting from the restoration of the ionic cross-links (Figure 7B). These findings are consistent with observations in DN hydrogels,[22,24,25,53] though, we observe much longer time-scales required for complete relaxation in our system. We believe that the enhanced relaxation times of these ionic cross-links are likely due to the nanoparticle-induced changes in the polymer segmental dynamics.

CONCLUSIONS

Although the responsive mechanism in ionic materials have been analyzed through several mechanistic approaches based on DN hydrogels, establishing the exact mechanism behind the ionic dissociation as well as delineating the key parameters responsible for the final material performance remain complex and challenging. In the present work, we proposed a fundamental understanding aiming at elucidating the underlying mechanisms behind the reversible breaking and reformation of ionic bonding in ionic organic−inorganic hybrids. The ionic nanocomposites leverage the reversible character of ionic bonds between imidazolium-functionalized polyurethanes and surface-modified sulfonate silica nanoparticles with the reinforcing effect of nanoparticles. Introducing ionic imidazolium-sulfonate interactions in the system led to the formation of an extended 3D network with unique property profile. First, introduction of either standard nonionic SiO_2 or ionic SiO_2−SO_3H into *im*-PU readily allowed us to precisely distinguish the contribution of the nanoparticle addition toward electrostatic interactions on mechanical performances, thermal transitions, morphology, and the crystallization process. Compared to the nonionic counterpart, the presence of reversible imidazolium-sulfonate interactions within ionic *im*-PU/SiO_2−SO_3H nanocomposite endowed the material with good nanoparticles dispersion, enhanced mechanical properties (i.e., yield stress, energy dissipation), and higher energy relaxation processes. Time−temperature superposition and dielectric spectroscopy permitted us to characterize the presence of ionic interactions and quantify relaxation modifications and cohesion improvement through determination of activation energies. The overall improved cohesion of the material through the incorporation of ionic interactions also modified the crystallization process. All these improvements appeared to be governed by two parameters: the dynamic and reversible nature of the electrostatic imidazolium-sulfonate interactions and the reduced mobility at the molecular level. The mechanistical approach confirmed the reversibility of the ionic cross-links allowing the material to restore after large deformation and resulting in energy dissipation following a unique strain-dependent behavior. Finally, loading−unloading cycles with holding time offers an interesting strategy to approach the dissociation kinetics of ionic interaction. Thereby, we brought, at least partially, a better understanding of the responsive mechanisms governing the superior performance origins of organic−inorganic ionic hybrids. We believe this work would inspire other authors to finely characterize ionic polymeric materials and design future ionic hybrids with adaptable properties.

ASSOCIATED CONTENT

Supporting Information

The Supporting Information is available free of charge at https://pubs.acs.org/doi/10.1021/acsapm.1c01396.

Shape−memory property, thermal recycling of *im*-PU/SiO_2−SO_3H; WLF/Arrhenius fitting comparison; SAXS under stretching; crystallization induction time, half-time, and spherulite growth rate; energy dissipation during loading/unloading cycles; and stress−strain curves for a conventional polypropylene composite (PDF)

AUTHOR INFORMATION

Corresponding Author

Jérémy Odent − *Laboratory of Polymeric and Composite Materials (LPCM), Center of Innovation and Research in Materials and Polymers (CIRMAP), University of Mons (UMONS), 7000 Mons, Belgium;* orcid.org/0000-0002-3038-846X; Email: jeremy.odent@umons.ac.be

Authors

Jean-Emile Potaufeux − *Laboratory of Polymeric and Composite Materials (LPCM), Center of Innovation and Research in Materials and Polymers (CIRMAP), University of Mons (UMONS), 7000 Mons, Belgium; Laboratory of*

https://doi.org/10.1021/acsapm.1c01396
ACS Appl. Polym. Mater. XXXX, XXX, XXX−XXX

Industrial and Human Automatic Control and Mechanical Engineering (LAMIH), UMR CNRS 8201, University Polytechnique Hauts-De-France (UPHF), Le Mont Houy 59313 Valenciennes, France

Delphine Notta-Cuvier − *Laboratory of Industrial and Human Automatic Control and Mechanical Engineering (LAMIH), UMR CNRS 8201, University Polytechnique Hauts-De-France (UPHF), Le Mont Houy 59313 Valenciennes, France*

Sophie Barrau − *CNRS, INRAE, Centrale Lille, UMR 8207 - UMET - Unité Matériaux et Transformations, Université de Lille, F-59000 Lille, France*

Chiara Magnani − *Laboratory of Polymeric and Composite Materials (LPCM), Center of Innovation and Research in Materials and Polymers (CIRMAP), University of Mons (UMONS), 7000 Mons, Belgium*

Rémi Delille − *Laboratory of Industrial and Human Automatic Control and Mechanical Engineering (LAMIH), UMR CNRS 8201, University Polytechnique Hauts-De-France (UPHF), Le Mont Houy 59313 Valenciennes, France*

Chunbo Zhang − *Beijing National Laboratory for Molecular Sciences, CAS Key Laboratory of Engineering Plastics, CAS Research/Education Center for Excellence in Molecular Sciences, Institute of Chemistry, Chinese Academy of Sciences, Beijing 100190, China;* orcid.org/0000-0002-6125-2207

Guoming Liu − *Beijing National Laboratory for Molecular Sciences, CAS Key Laboratory of Engineering Plastics, CAS Research/Education Center for Excellence in Molecular Sciences, Institute of Chemistry, Chinese Academy of Sciences, Beijing 100190, China;* orcid.org/0000-0003-2808-2661

Emmanuel P. Giannelis − *Department of Materials Science and Engineering, Cornell University, Ithaca, New York 14853, United States*

Alejandro J. Müller − *POLYMAT and Department of Polymers and Advanced Materials: Physics, Chemistry and Technology, Faculty of Chemistry, University of the Basque Country UPV/EHU, Donostia-San Sebastián 20018, Spain; IKERBASQUE, Basque Foundation for Science, Bilbao 48009, Spain;* orcid.org/0000-0001-7009-7715

Franck Lauro − *Laboratory of Industrial and Human Automatic Control and Mechanical Engineering (LAMIH), UMR CNRS 8201, University Polytechnique Hauts-De-France (UPHF), Le Mont Houy 59313 Valenciennes, France*

Jean-Marie Raquez − *Laboratory of Polymeric and Composite Materials (LPCM), Center of Innovation and Research in Materials and Polymers (CIRMAP), University of Mons (UMONS), 7000 Mons, Belgium;* orcid.org/0000-0003-1940-7129

Complete contact information is available at: https://pubs.acs.org/10.1021/acsapm.1c01396

Author Contributions

The manuscript was written through contributions of all authors. All authors have given approval to the final version of the manuscript.

Notes

The authors declare no competing financial interest.

■ ACKNOWLEDGMENTS

The authors gratefully acknowledge support from both the Wallonia and the European Commission "FSE and FEDER" in the frame of LCFM-BIOMASS project as well as the National Fund for Scientific Research (F.R.S.-FNRS). We would like to thank the financial support provided by the BIODEST project. This project has received funding from the European Union's Horizon 2020 research and innovation program under the Marie Sklodowska-Curie Grant Agreement No. 778092. J.-M.R. is "Chercheur qualifié" by the F.R.S.-F.N.R.S. A.J.M. would like to acknowledge funding from the Basque Government through Grant IT1309-19. LAMIH authors are grateful to CISIT, the Hauts de France Region, the European Community, the Regional Delegation for Research and Technology, the Ministry of Higher Education and Research, and the National Center for Scientific Research for their financial support.

■ REFERENCES

(1) Lehn, J.-M. Dynamers: dynamic molecular and supramolecular polymers. *Prog. Polym. Sci.* **2005**, *30* (8−9), 814−831.

(2) Cavicchi, K. A.; Pantoja, M.; Cakmak, M. Shape memory ionomers. *J. Polym. Sci., Part B: Polym. Phys.* **2016**, *54* (14), 1389−1396.

(3) Hornat, C. C.; Urban, M. W. Shape memory effects in self-healing polymers. *Prog. Polym. Sci.* **2020**, *102*, 101208.

(4) Hu, L.; Zhang, Q.; Li, X.; Serpe, M. J. Stimuli-responsive polymers for sensing and actuation. *Mater. Horiz.* **2019**, *6* (9), 1774−1793.

(5) Zhang, L.; Liu, Z.; Wu, X.; Guan, Q.; Chen, S.; Sun, L.; Guo, Y.; Wang, S.; Song, J.; Jeffries, E. M.; He, C.; Qing, F.-L.; Bao, X.; You, Z. A Highly Efficient Self-Healing Elastomer with Unprecedented Mechanical Properties. *Adv. Mater.* **2019**, *31* (23), 1901402.

(6) Liu, Z.; Zhang, L.; Guan, Q.; Guo, Y.; Lou, J.; Lei, D.; Wang, S.; Chen, S.; Sun, L.; Xuan, H.; Jeffries, E. M.; He, C.; Qing, F.-L.; You, Z. Biomimetic Materials with Multiple Protective Functionalities. *Adv. Funct. Mater.* **2019**, *29* (28), 1901058.

(7) Liu, H.; Xiong, C.; Tao, Z.; Fan, Y.; Tang, X.; Yang, H. Zwitterionic copolymer-based and hydrogen bonding-strengthened self-healing hydrogel. *RSC Adv.* **2015**, *5* (42), 33083−33088.

(8) Shinde, S.; Sartucci, J. L.; Jones, D. K.; Gavvalapalli, N. Dynamic π-Conjugated Polymer Ionic Networks. *Macromolecules* **2017**, *50* (19), 7577−7583.

(9) Liu, J.; Liu, Y.; Wang, Y.; Zhu, J.; Yu, J.; Hu, Z. Disulfide bonds and metal-ligand co-crosslinked network with improved mechanical and self-healing properties. *Materials Today Communications* **2017**, *13*, 282−289.

(10) Bose, R. K.; Hohlbein, N.; Garcia, S. J.; Schmidt, A. M.; van der Zwaag, S. Connecting supramolecular bond lifetime and network mobility for scratch healing in poly(butyl acrylate) ionomers containing sodium, zinc and cobalt. *Phys. Chem. Chem. Phys.* **2015**, *17* (3), 1697−1704.

(11) Hui, Y.; Wen, Z.-B.; Pilate, F.; Xie, H.; Fan, C.-J.; Du, L.; Liu, D.; Yang, K.-K.; Wang, Y.-Z. A facile strategy to fabricate highly-stretchable self-healing poly(vinyl alcohol) hybrid hydrogels based on metal-ligand interactions and hydrogen bonding. *Polym. Chem.* **2016**, *7* (47), 7269−7277.

(12) Su, E.; Okay, O. Polyampholyte hydrogels formed via electrostatic and hydrophobic interactions. *Eur. Polym. J.* **2017**, *88*, 191−204.

(13) Pluth, M. D.; Raymond, K. N. Reversible guest exchange mechanisms in supramolecular host-guest assemblies. *Chem. Soc. Rev.* **2007**, *36* (2), 161−171.

(14) Chen, Q.; Yan, X.; Zhu, L.; Chen, H.; Jiang, B.; Wei, D.; Huang, L.; Yang, J.; Liu, B.; Zheng, J. Improvement of Mechanical Strength and Fatigue Resistance of Double Network Hydrogels by Ionic Coordination Interactions. *Chem. Mater.* **2016**, *28* (16), 5710−5720.

(15) Comí, M.; Lligadas, G.; Ronda, J. C.; Galià, M.; Cádiz, V. Adaptive bio-based polyurethane elastomers engineered by ionic hydrogen bonding interactions. *Eur. Polym. J.* **2017**, *91*, 408−419.

(16) Keplinger, C.; Sun, J. Y.; Foo, C. C.; Rothemund, P.; Whitesides, G. M.; Suo, Z. Stretchable, Transparent, Ionic Conductors. *Science* **2013**, *341* (6149), 984−987.
(17) Potaufeux, J.-E.; Odent, J.; Notta-Cuvier, D.; Lauro, F.; Raquez, J.-M. A comprehensive review of the structures and properties of ionic polymeric materials. *Polym. Chem.* **2020**, *11* (37), 5914−5936.
(18) Capek, I. Nature and properties of ionomer assemblies. II. *Adv. Colloid Interface Sci.* **2005**, *118* (1−3), 73−112.
(19) Blackman, L. D.; Gunatillake, P. A.; Cass, P.; Locock, K. E. S. An introduction to zwitterionic polymer behavior and applications in solution and at surfaces. *Chem. Soc. Rev.* **2019**, *48* (3), 757−770.
(20) Mayumi, K.; Marcellan, A.; Ducouret, G.; Creton, C.; Narita, T. Stress-Strain Relationship of Highly Stretchable Dual Cross-Link Gels: Separability of Strain and Time Effect. *ACS Macro Lett.* **2013**, *2* (12), 1065−1068.
(21) Morovati, V.; Dargazany, R. Micro-mechanical modeling of the stress softening in double-network hydrogels. *Int. J. Solids Struct.* **2019**, *164*, 1−11.
(22) Lu, H.; Wang, X.; Shi, X.; Yu, K.; Fu, Y. Q. A phenomenological model for dynamic response of double-network hydrogel composite undergoing transient transition. *Composites, Part B* **2018**, *151*, 148−153.
(23) Hui, C.-Y.; Long, R. A constitutive model for the large deformation of a self-healing gel. *Soft Matter* **2012**, *8* (31), 8209.
(24) Long, R.; Mayumi, K.; Creton, C.; Narita, T.; Hui, C.-Y. Time Dependent Behavior of a Dual Cross-Link Self-Healing Gel: Theory and Experiments. *Macromolecules* **2014**, *47* (20), 7243−7250.
(25) Mao, Y.; Lin, S.; Zhao, X.; Anand, L. A large deformation viscoelastic model for double-network hydrogels. *J. Mech. Phys. Solids* **2017**, *100*, 103−130.
(26) Külcü, İ. D. Characterization of stress softening and self-healing in a double network hydrogel. *Results Phys.* **2019**, *12*, 1826−1833.
(27) Bacca, M.; Creton, C.; McMeeking, R. M. A Model for the Mullins Effect in Multinetwork Elastomers. *J. Appl. Mech.* **2017**, *84* (12), 121009.
(28) Odent, J.; Raquez, J. M.; Dubois, P.; Giannelis, E. P. Ultra-stretchable ionic nanocomposites: from dynamic bonding to multi-responsive behavior. *J. Mater. Chem. A* **2017**, *5* (26), 13357−13363.
(29) Potaufeux, J.-E.; Odent, J.; Notta-Cuvier, D.; Delille, R.; Barrau, S.; Giannelis, E. P.; Lauro, F.; Raquez, J.-M. Mechanistic insights on ultra-tough polylactide-based ionic nanocomposites. *Compos. Sci. Technol.* **2020**, *191*, 108075.
(30) Odent, J.; Raquez, J.-M.; Samuel, C.; Barrau, S.; Enotiadis, A.; Dubois, P.; Giannelis, E. P. Shape-Memory Behavior of Polylactide/Silica Ionic Hybrids. *Macromolecules* **2017**, *50* (7), 2896−2905.
(31) Li, G.; Wang, A. Cold, warm, and hot programming of shape memory polymers. *J. Polym. Sci., Part B: Polym. Phys.* **2016**, *54* (14), 1319−1339.
(32) Liu, C.-Y.; He, J.; Keunings, R.; Bailly, C. New Linearized Relation for the Universal Viscosity-Temperature Behavior of Polymer Melts. *Macromolecules* **2006**, *39* (25), 8867−8869.
(33) Williams, M. L.; Landel, R. F.; Ferry, J. D. The Temperature Dependence of Relaxation Mechanisms in Amorphous Polymers and Other Glass-forming Liquids. *J. Am. Chem. Soc.* **1955**, *77* (14), 3701−3707.
(34) Li, Z.; Wu, Z.; Mo, G.; Xing, X.; Liu, P. A Small-Angle X-Ray Scattering Station At Beijing Synchrotron Radiation Facility. *Instrum. Sci. Technol.* **2014**, *42* (2), 128−141.
(35) Menon, S. V. G.; Manohar, C.; Rao, K. S. A new interpretation of the sticky hard sphere model. *J. Chem. Phys.* **1991**, *95* (12), 9186−9190.
(36) Sutton, M. A.; Orteu, J.-J.; Schreier, H. W. *Image correlation for shape, motion and deformation measurements: basic concepts, theory and applications*; Springer: New York, 2009; Vol. *1*, pp 1−322.
(37) Block, C.; Watzeels, N.; Rahier, H.; Van Mele, B.; Van Assche, G. Rheology of nanocomposites: Modelling and interpretation of nanofiller influence. *J. Therm. Anal. Calorim.* **2011**, *105* (2), 731−736.
(38) Van Gurp, M.; Palmen, J. Time-temperature superposition for polymeric blends. *Rheol. Bull.* **1998**, *67*, 5−8.
(39) Bohn, M. A. The Connection Between the Parameters of WLF Equation and of Arrhenius Equation. *Propellants, Explos., Pyrotech.* **2019**, *44* (6), 696−705.
(40) Suarez-Martinez, P. C.; Batys, P.; Sammalkorpi, M.; Lutkenhaus, J. L. Time-Temperature and Time-Water Superposition Principles Applied to Poly(allylamine)/Poly(acrylic acid) Complexes. *Macromolecules* **2019**, *52* (8), 3066−3074.
(41) Kudlik, A.; Benkhof, S.; Blochowicz, T.; Tschirwitz, C.; Rössler, E. The dielectric response of simple organic glass formers. *J. Mol. Struct.* **1999**, *479* (2−3), 201−218.
(42) Körber, T.; Mohamed, F.; Hofmann, M.; Lichtinger, A.; Willner, L.; Rössler, E. A. The Nature of Secondary Relaxations: The Case of Poly(ethylene- *alt* -propylene) Studied by Dielectric and Deuteron NMR Spectroscopy. *Macromolecules* **2017**, *50* (4), 1554−1568.
(43) Ding, Y.; Pawlus, S.; Sokolov, A. P.; Douglas, J. F.; Karim, A.; Soles, C. L. Dielectric Spectroscopy Investigation of Relaxation in C_{60} -Polyisoprene Nanocomposites. *Macromolecules* **2009**, *42* (8), 3201−3206.
(44) Mohamed, F.; Hameed, T. A.; Abdelghany, A. M.; Turky, G. Structure-dynamic properties relationships in poly(ethylene oxide)/silicon dioxide nanocomposites: dielectric relaxation study. *Polym. Bull.* **2021**, *78*, 5205−5223.
(45) Se, K.; Adachi, K.; Kotaka, T. Dielectric Relaxations in Poly(ethylene oxide): Dependence on Molecular Weight. *Polym. J.* **1981**, *13* (11), 1009−1017.
(46) Jimenez, A. M.; Krauskopf, A. A.; Pérez-Camargo, R. A.; Zhao, D.; Pribyl, J.; Jestin, J.; Benicewicz, B. C.; Müller, A. J.; Kumar, S. K. Effects of Hairy Nanoparticles on Polymer Crystallization Kinetics. *Macromolecules* **2019**, *52* (23), 9186−9198.
(47) Zhao, W.; Su, Y.; Gao, X.; Xu, J.; Wang, D. Interfacial effect on confined crystallization of poly(ethylene oxide)/silica composites. *J. Polym. Sci., Part B: Polym. Phys.* **2016**, *54* (3), 414−423.
(48) Guerre, M.; Taplan, C.; Winne, J. M.; Du Prez, F. E. Vitrimers: directing chemical reactivity to control material properties. *Chemical Science* **2020**, *11* (19), 4855−4870.
(49) Lamers, B. A. G.; Ślęczkowski, M. L.; Wouters, F.; Engels, T. A. P.; Meijer, E. W.; Palmans, A. R. A. Tuning polymer properties of non-covalent crosslinked PDMS by varying supramolecular interaction strength. *Polym. Chem.* **2020**, *11* (16), 2847−2854.
(50) Sun, T. L.; Kurokawa, T.; Kuroda, S.; Ihsan, A. B.; Akasaki, T.; Sato, K.; Haque, M. A.; Nakajima, T.; Gong, J. P. Physical hydrogels composed of polyampholytes demonstrate high toughness and viscoelasticity. *Nat. Mater.* **2013**, *12* (10), 932−937.
(51) Deschanel, S.; Greviskes, B. P.; Bertoldi, K.; Sarva, S. S.; Chen, W.; Samuels, S. L.; Cohen, R. E.; Boyce, M. C. Rate dependent finite deformation stress-strain behavior of an ethylene methacrylic acid copolymer and an ethylene methacrylic acid butyl acrylate copolymer. *Polymer* **2009**, *50* (1), 227−235.
(52) Cui, K.; Sun, T. L.; Kurokawa, T.; Nakajima, T.; Nonoyama, T.; Chen, L.; Gong, J. P. Stretching-induced ion complexation in physical polyampholyte hydrogels. *Soft Matter* **2016**, *12* (43), 8833−8840.
(53) Drozdov, A. D.; deClaville Christiansen, J. Double-network gels with dynamic bonds under multi-cycle deformation. *Journal of the Mechanical Behavior of Biomedical Materials* **2018**, *88*, 58−68.
(54) Shah, D.; Maiti, P.; Jiang, D. D.; Batt, C. A.; Giannelis, E. P. Effect of Nanoparticle Mobility on Toughness of Polymer Nanocomposites. *Adv. Mater.* **2005**, *17* (5), 525−528.
(55) Gersappe, D. Molecular Mechanisms of Failure in Polymer Nanocomposites. *Phys. Rev. Lett.* **2002**, *89* (5), 058301.

https://doi.org/10.1021/acsapm.1c01396
ACS Appl. Polym. Mater. XXXX, XXX, XXX−XXX